ARTICLE

# Kinetics of Thermal Decomposition of Lithium Hexafluorophosphate

Xiao-min Liu*, Hui Yang

*College of Materials Science and Engineering, Nanjing University of Technology, Nanjing 210009, China*

(Dated: Received on March 12, 2013; Accepted on May 3, 2013)

With on-line coupled thermo-gravimetric analyzer-Fourier transform infrared spectrometer technique, the thermal decomposition of lithium hexafluorophosphate ($LiPF_6$) and its gas evolution at inert environment ($H_2O$<10 ppm) were studied under both non-isothermal and isothermal conditions. The results showed that the $LiPF_6$ decomposition is a single-stage reaction with LiF as final residue and $PF_5$ as gas product. In addition, its decomposition kinetics was determined as 2D phase boundary movement (cylindrical symmetry) under both non-isothermal and isothermal conditions. Furthermore, the activation energy of $LiPF_6$ decomposition was calculated as 104 and 92 kJ/mol for non-isothermal and isothermal conditions, respectively.

**Key words:** Lithium hexafluorophosphate, Decomposition kinetics, Online coupled thermo-gravimetric analyzer-Fourier transform infrared spectrometer

## I. INTRODUCTION

Lithium hexafluorophosphate is the most widely employed salt in the electrolyte used in commercial Li-ion cells due to many advantages such as its high ion conductivity in organic solutions and its electrochemical stability, *etc.* However, its thermal instability decomposing to $PF_5$ gas [1] was claimed to affect the electrolyte chemistry and hence influenced the electrochemical behavior [2], caused the cell gassing when being stored at elevated temperature [3]. In addition, its poor hydrolytic stability reacting with moisture to yield HF, was detrimental to the cycling performance of $LiMn_2O_4$ [4, 5] and $LiCoPO_4$ [6]. Many studies have been carried out to investigate the thermal behaviors of $LiPF_6$ under various conditions [1, 2, 6−15]. Wang *et al.* [8] and Lekgoathi *et al.* [13] studied the decomposition kinetics of the $LiPF_6$ and calculated the activation energy and pre-exponential factor. With on-line coupled thermo-gravimetric analyzer-Fourier transform infrared spectrometer (TGA-FTIR) technique, Yang *et al.* characterized the thermal stability and gases evolution of neat $LiPF_6$ and $LiPF_6$ based electrolyte [9]. Wilken *et al.* [14] and Arbizzani *et al.* [15] also studied the thermal stability of $LiPF_6$ based electrolyte via different techniques.

In this work, with the same technique for the first time the decomposition model of the neat $LiPF_6$ was determined as 2D phase boundary movement under both isothermal and non-isothermal conditions, which is of great importance for the further study of the thermal decomposition characteristics of $LiPF_6$ in electrolyte/practical batteries, and put some important insight into the simulation of thermal runaway of the lithium ion cell as well as in safety prediction of lithium ion batteries.

## II. EXPERIMENTS

$LiPF_6$ sample was provided by Aldrich (99%) and used as received. Thermo-gravimetric measurements were performed with TGA model 2960. The TGA was modified and its inert working condition was checked with copper oxalate according to the work of Mullens *et al.* [18]. In addition, the TGA was covered with a glove bag which was continuously purged with Argon in all the experiments. Samples were transferred from Ar atmosphere dry box ($H_2O$<10 ppm) to this glove bag with a vacuum carrier. All the experiments were performed in dynamic atmospheres (40 mL/min) of Ar. The non-isothermal analyses were carried out at various heating rates (2.5, 5, 10, and 20 °C/min), while the isothermal analyses were carried out at constant temperatures (110, 130, 150, 170, and 190 °C) for 1 h. The TGA was on-line coupled with a gas inter-phase FTIR spectrometer in order to identify the evolved gas. In all experiments, a resolution of 4 $cm^{-1}$ was selected for the FTIR detector. FTIR was also covered with another glove bag which was filled with nitrogen from the purge gas of IR itself to eliminate the artifacts of the moisture and $CO_2$ from the air. The outlet of TGA was connected to FTIR with a heating tube maintaining at 200 °C in all experiments.

## III. RESULTS AND DISCUSSION

Thermogravimetry (TG) profile of pure $LiPF_6$ salt, obtained at a heating rate of 10 °C/min, and in the

*Author to whom correspondence should be addressed. E-mail: lxm3799@yahoo.com, Tel./FAX: +86-25-83587275

 

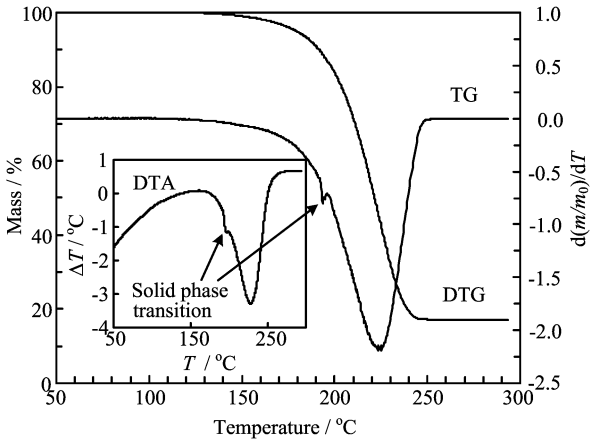


FIG. 1 Mass loss (TG), derivation of mass loss (DTG) and DTA curve (inset) for thermal decompositions of $LiPF_6$ in Argon (40 mL/min) with a heating rate of 10 °C/min carried out with TGA setup.

40 mL/min Ar carrier gas containing less than 10 ppm of $H_2O$, is presented in Fig.1. The mass of remaining solid residue is about 17% when the temperature reaches 300 °C. As shown in derivative thermal analysis (DTA) trace (inset plot), the thermal decomposition of $LiPF_6$ is an endothermic process with the decomposition enthalpy of 84.27 kJ/mol [4]. A small endothermic peak at ∼200 °C superposing on the main peak can be attributed to the solid-phase transformation of $LiPF_6$ based on observation of an endothermic peak at similar temperature by differential scanning calometry [16]. This phase transformation enthalpy is reported to be 2.61±0.03 kJ/mol [5].

To investigate the gaseous product of $LiPF_6$ during its thermal decomposition, the evolution of gas products as a result of sample thermal decomposition or volatilization was simultaneously monitored by FTIR during TGA experiment. The infrared spectra collected in the stacked plot of Fig.2(a) clearly show that $PF_5$ is the only gaseous product during the $LiPF_6$ decomposition. As shown in the extracted spectrum Fig.2(b), the spectral features of strong intensity are observed at 1018 and 975 $cm^{-1}$, along with weak features at 586 and 534 $cm^{-1}$. Molecular orbital (MO) calculation reveals that there are two chemically nonequivalent fluorine, denoted as F(1) and F(2) in $PF_5$. Stretching and bending modes of F(1)P are located at 1018 and 586 $cm^{-1}$, respectively, while those of F(2)P are at 945 and 534 $cm^{-1}$. The shift of stretching and bending mode of towards lower wavenumber indicates the F(2)P bond strength is weaker than its counterpart.

As shown in Fig.2(a), $PF_5$ is the only gas phase product detected by FTIR in the temperature range of 110−300 °C. Meanwhile, the weight percent of the remaining solid residue at the end of TG analysis was 17% of the initial mass (Fig.1), in good agreement with calculated lithium fluoride (LiF) to $LiPF_6$ mass ratio,

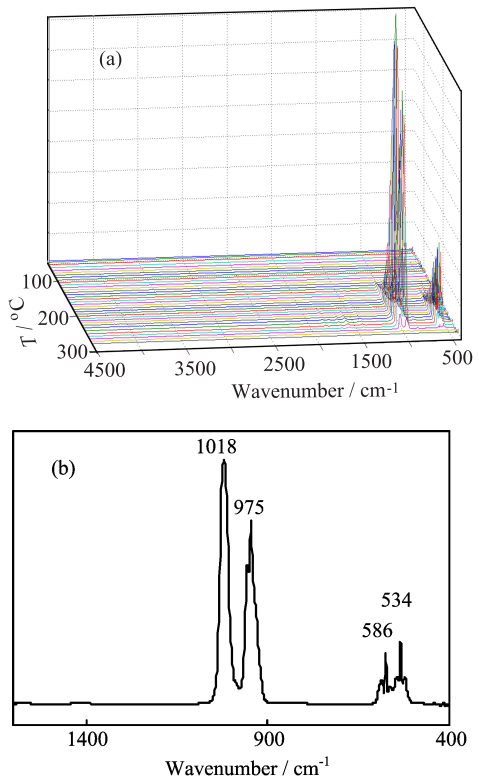


FIG. 2 (a) The 3D plot for the FTIR spectra of the evolved gases produced by the thermal decomposition of $LiPF_6$ (heating rate of 10 °C/min, Ar flow rate of 40 mL/min). (b) FTIR spectrum extracted at 205 °C from (a).

therefore, the reaction path can be clearly presented as

$$LiPF_6 \rightarrow LiF + PF_5 \tag{1}$$

The thermal decompositions of $LiPF_6$ at different heat ramping rates, 2.5, 5, 10, and 20 °C/min were carried out to explore the kinetics of this reaction in the non-isothermal condition. The degree of decomposition, $\alpha$, is plotted in Fig.3 as a function of temperature. $\alpha$ was calculated as fraction $\alpha=\Delta m_t/\Delta m$, where $\Delta m_t$ represents the mass loss after time $t$ respect to the initial mass $m_0$ and $\Delta m$ is the total mass loss when the decomposition is complete. The kinetics parameters of a non-isothermal reaction is determined by using the following differential kinetics equation:

$$\frac{\mathrm{d}\alpha}{\mathrm{dt}} = A\exp\left(\frac{-E_a}{RT}\right) f(\alpha) \tag{2}$$

where $f(\alpha)$ is a function of $\alpha$ depending on a kinetics model (*i.e.* on a mechanism of reaction), $E_a$ is the activation energy, $R$ is the gas constant, and $A$ is the frequency factor. The above equation can be rewritten as

$$\ln\left[\frac{\mathrm{d}\alpha}{\mathrm{d}t}\frac{1}{f(\alpha)}\right] = -\frac{E_a}{RT} + \ln A \tag{3}$$

DOI:10.1063/1674-0068/26/04/467-470 

TABLE I Kinetics expression of for solid-state reactions.

| Rate determining mechanism | $f(\alpha)$ | $g(\alpha)$ |
|---|---|---|
| Mampel unimolecular law | $1-\alpha$ | $-\ln(1-\alpha)$ |
| Avrami-Erofeev nuclei growth–2D | $2(1-\alpha)[-\ln(1-\alpha)]^{1/2}$ | $[-\ln(1-\alpha)]^{1/2}$ |
| Avrami-Erofeev nuclei growth–3D | $3(1-\alpha)[-\ln(1-\alpha)]^{1/2}$ | $[-\ln(1-\alpha)]^{1/3}$ |
| Prout-Tomphkins branching nuclei | $\alpha(1-\alpha)$ | $\ln[(\alpha/(1-\alpha)]$ |
| Parabolic law–1D | $\alpha^{-1}$ | $\alpha^2/2$ |
| 2D diffusion | $[-\ln(1-\alpha)]^{-1}$ | $(1-\alpha)\ln(1-\alpha)+\alpha$ |
| 3D spherical diffusion (Jander) | $(1-\alpha)^{2/3}[(1-\alpha)^{-1/3}-1]^{-1}$ | $1.5[1-(1-\alpha)^{1/3}]^2$ |
| 3D spherical diffusion (Brounshtein Ginstling) | $[(1-\alpha)^{-1/3}-1]^{-1}$ | $1.5[1-2\alpha/3-(1-\alpha)^{2/3}]$ |
| 1D phase boundary movement (zero order) constant | Constant | $\alpha$ |
| 2D phase boundary movement (cylindrical symmetry) | $(1-\alpha)^{1/2}$ | $2[1-(1-\alpha)^{1/2}]$ |
| 3D phase boundary movement (spherical symmetry) | $(1-\alpha)^{2/3}$ | $3[1-(1-\alpha)^{1/3}]$ |
| Power law | $(1-\alpha)^n$ | $[1-(1-\alpha)^{1-n}]/(1-n)$ |

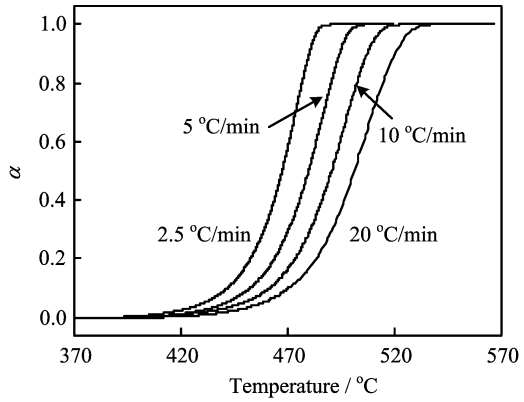


FIG. 3 $\alpha$(t) plots for non-isothermal decomposition of $LiPF_6$ with different heating rates.

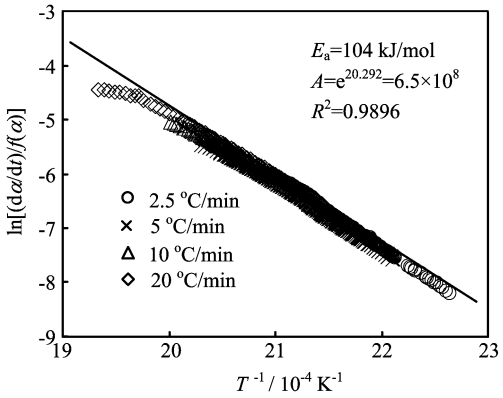


FIG. 4 $\ln\left[\frac{d\alpha}{dt}\frac{1}{f(\alpha)}\right]$ *vs.* $1/T$ plot where $f(\alpha)$ employs the 2D phase movement equation.

Thus the plots of $\ln\left[\frac{d\alpha}{dt}\frac{1}{f(\alpha)}\right]$ *vs.* $1/T$ should be independent of the heating rate but fit in the same linear line if the correct form of $f(\alpha)$ is chosen. The $E_a$ and $A$ can be obtained from the slope and the intercept of such plot. The possible kinetics expressions for $f(\alpha)$ can be derived from various physical situations and examples are given in Table I [17]. In our case, the cylindrical symmetry phase boundary movement model ($(1-\alpha)^{1/2}$) gave the best fit to the experiment data as shown in Fig.4. The activation energy for the decomposition of $LiPF_6$ is 104 kJ/mol and the frequency constant is $6.5\times10^8$ which are in good agreement with the reported data [6, 13]. The kinetics information can also be extracted from the isothermal experiments carried out at different temperatures. In the isothermal condition at temperature $T_0$, Eq.(1) can be rewritten as

$$\frac{d\alpha}{f(\alpha)} = A\exp\left(\frac{-E_a}{RT_0}\right)dt \tag{4}$$

In the integral form

$$\begin{aligned} g(\alpha) &\equiv \int_0^\alpha \frac{d\alpha}{f(\alpha)} \\ &= \int_0^t A\exp\left(\frac{-E_a}{RT_0}\right)dt \\ &= A\exp\left(\frac{-E_a}{RT_0}\right)t \\ &= k_0 t \end{aligned} \tag{5}$$

Thus the plot of $g(\alpha)$ versus time of experiment carried out at constant temperature $T_0$ should be linear if correct $g(\alpha)$ is chosen. The isothermal experiments were carried out at 110, 130, 150, 170, and 190 °C, respectively. Different $g(\alpha)$ equations from Table I were used to fit the experiments data. It was found that the 2D phase boundary movement equation, the same one obtained in the non-isothermal experiments, gave the best fit in the isothermal conditions. The values of $k_0$ calculated at different temperatures are listed in Table II. Furthermore, the activation energy and fre-

DOI:10.1063/1674-0068/26/04/467-470 

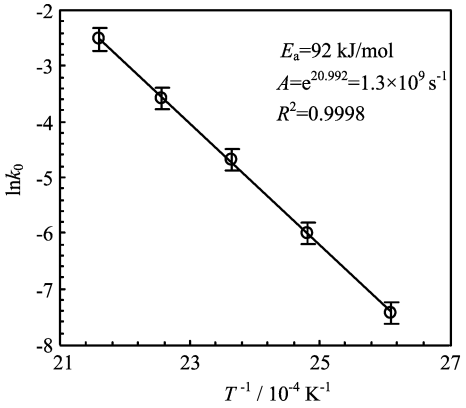


FIG. 5 ln$k_0$ *vs.* $1/T$ plot under the isothermal condition.

TABLE II Estimated $k_0$ of Eq.(4) for isothermal experiments based on 2D phase boundary movement model.

| $T$/°C | $T^{-1}/10^{-4}K^{-1}$ | $k_0/10^{-4}$ s$^{-1}$ | $R^2$ |
|---|---|---|---|
| 110 | 26.10 | 6.0106 | 0.9999 |
| 130 | 24.81 | 25.156 | 0.9980 |
| 150 | 23.63 | 93.357 | 0.9995 |
| 170 | 22.57 | 334.61 | 0.9982 |
| 190 | 21.59 | 817.76 | 0.9987 |

quency factor can be calculated from the slope and intercepted by plotting ln$k_0$ *vs.* $1/T$ as shown in Fig.5. In the isothermal condition, the activation energy is 92 kJ/mol and the frequency factor is $1.3\times10^9$. The activation energy obtained at isothermal condition is shown ∼10% deviation from that calculated from non-isothermal measurements. In conclusion, it can be stated that the kinetics of the $LiPF_6$ decomposition proceed with the same mechanism in both isothermal and non-isothermal conditions.

## IV. CONCLUSION

The thermal decomposition of Lithium Hexafluorophosphate ($LiPF_6$) and its gas evolution at inert environment ($H_2O$<10 ppm) were studied on-line coupled TGA-FTIR technique under both non-isothermal and isothermal conditions. Decomposition of $LiPF_6$ in inert atmosphere is a simple, and one-stage reaction leading to LiF as solid and $PF_5$ as gaseous products. In addition, this decomposition follows the 2D phase boundary movement model ($(1-\alpha)^{1/2}$) with the activation energy calculated as 98±6 kJ/mol.

## V. ACKNOWLEDGMENTS

This work was supported by the National Natural Science Foundation of China (No.20803035) and the Priority Academic Program Development of Jiangsu Higher Education Institutions.

[1] A. V. Plakhotnyk, L. Ernst, and R. Schmutzler, J. Fluorine Chem. **126**, 27 (2005).
[2] S. E. Sloop, J. K. Pugh, S. Wang, J. B. Kerr, and K. Kinoshita, Electrochem. Solid-State Lett. **4**, A42 (2001).
[3] H. H. Lee, C. C. Wan, and Y. Y. Wang, J. Electrochem. Soc. **151**, A542 (2004).
[4] D. H. Jang, Y. J. Shin, and S. M. Oh, J. Electrochem. Soc. **143**, 2204 (1996).
[5] N. S. Choi, J. T. Yeon, Y. W. Lee, J. G. Han, K. T. Lee, and S. S. Kim, Solid State Ionics **219**, 41 (2012).
[6] R. Sharabi, E. Markevich, V. Borgel, G. Salitra, G. Gershinsky, D. Aurbach, G. Semrau, M. A. Schmidt, N. Schall, and C. Stinner, J. Power Sources **203**, 109 (2012).
[7] K. S. Gavritchev, G. A. Sharpataya, A. A. Smagin, E. N. Malyi, and V. A. Matyukha, J. Thermal Anal. Calorimetry **73**, 71 (2003).
[8] Q. S. Wang, J. H. Sun, S. X. Lu, X. L. Yao, and C. H. Chen, Solid State Ionics **177**, 137 (2006).
[9] H. Yang, G. V. Zhuang, and P. N. Ross, J. Power Sources **161**, 573 (2007).
[10] X. G. Teng, F. Q. Li, P. H. Ma, Q. D. Ren, and S. Y. Li, Thermochim. Acta **436**, 30 (2005).
[11] E. Zinigrad, L. Larush-Asraf, J. S. Gnanaraj, M. Sprecher, and D. Aurbach, Thermochim. Acta **438**, 184 (2005).
[12] H. Yang and X. D. Shen, J. Power Sources **167**, 515 (2007).
[13] M. D. S. Lekgoathi, B. M. Vilakazi, J. B. Wagener, J. P. Le Roux, and D. Moolman, J. Fluorine Chem. **149**, 53 (2013).
[14] S. Wilken, P. Johansson, and P. Jacobsson, Solid State Ionics **225**, 608 (2012).
[15] C. Arbizzani, G. Gabrielli, and M. Mastragostino, J. Power Sources **196**, 4801 (2011).
[16] B. Ravdel, K. M. Abraham, R. Gitzendanner, J. DiCarlo, B. Lucht, and C. Campion, J. Power Sources **119-121**, 805 (2003).
[17] L. N. Dinh, C. M. Cecala, J. H. Leckey, and M. Balooch, J. Nuclear Mater. **295**, 193 (2001).
[18] J. Mullens, A. Vos, R. Carleer, J. Yperman, and L. C. Van Poucke, Thermochim. Acta **207**, 337 (1992).

DOI:10.1063/1674-0068/26/04/467-470 